Observation of Sub-Microsecond Protein Methyl-Side Chain Dynamics by Nanoparticle-Assisted NMR Spin Relaxation

Xinyao Xiang,[1] Alexandar L. Hansen,[2] Lei Yu,[1] Gregory Jameson,[1] Lei Bruschweiler-Li,[2]

Chunhua Yuan,[2] and Rafael Brüschweiler[1,2,3*]

[1]Department of Chemistry and Biochemistry, The Ohio State University, Columbus, Ohio 43210, United States

[2]Campus Chemical Instrument Center, The Ohio State University, Columbus, Ohio 43210, United States

[3]Department of Biological Chemistry and Pharmacology, The Ohio State University, Columbus, Ohio 43210, United States

[*]To whom correspondence should be addressed:

Rafael Brüschweiler, Ph.D.

Department of Chemistry and Biochemistry, Room 382 CBEC,

151 W. Woodward Ave, The Ohio State University, Columbus, Ohio 43210

E-mail: bruschweiler.1@osu.edu

Abstract

Amino-acid side-chain properties in proteins are key determinants of protein function. NMR spin relaxation of side chains is an important source of information about local protein dynamics and flexibility. However, traditional solution NMR relaxation methods are most sensitive to sub-nanosecond dynamics lacking information on slower ns-μs timescale motions. Nanoparticle-assisted NMR spin relaxation (NASR) of methyl-side chains is introduced here as a window into these ns-μs dynamics. NASR utilizes the transient and non-specific interactions between folded proteins and slowly tumbling spherical nanoparticles (NPs), whereby the increase of the relaxation rates reflects motions on timescales from ps all the way to the overall tumbling correlation time of the NPs ranging from hundreds of ns to μs. The observed motional amplitude of each methyl group can then be expressed by a model-free order parameter S^2(NASR). The method is demonstrated for ^{2}H-relaxation of CH_2D methyl moieties and cross-correlated relaxation of CH_3 groups for proteins Im7 and ubiquitin in the presence of anionic silica-nanoparticles. Both types of relaxation experiments, dominated by either quadrupolar or dipolar interactions, yield highly consistent results. Im7 shows additional dynamics on the intermediate timescales taking place in a functionally important loop, whereas ubiquitin visits the majority of its conformational substates on the sub-ns timescale. These experimental observations are in good agreement with 4-10 μs all-atom molecular dynamics trajectories. NASR probes side-chain dynamics on a much wider range of motional timescales than previously possible, thereby providing new insights into the interplay between protein structure, dynamics, and molecular interactions that govern protein function.

Keywords: Protein methyl groups, side-chain dynamics, NMR spin relaxation, silica nanoparticles, molecular dynamics.

Introduction

The many specific biochemical functions performed by a manifold of different proteins is a consequence of the diverse chemical and biophysical nature of their amino-acid side chains. Amino-acid side chains allow many different types of intramolecular and intermolecular interactions, which are enabled and modulated by variable degrees of side-chain dynamics.[1] Among all amino acids, methyl-bearing residues are unique as they are frequently present in the hydrophobic protein core and at interfaces. It has been shown how methyl groups can play important roles in mediating protein stability and function, including folding,[2] allostery,[3] molecular recognition, and protein-ligand interactions.[4-6]

Due to their favorable nuclear spin properties, methyl groups have become widely used probes for protein dynamics studies using nuclear magnetic resonance (NMR). In fact, besides backbone amide N-H groups, methyl groups are the most widely used moieties studied by solution protein NMR providing atomic-detail information about dynamics on multiple timescales.[1, 7] For this purpose, an array of sophisticated solution NMR experiments has been developed. Methyl groups are particularly advantageous for NMR studies of proteins and their complexes that have high molecular weights, since the rapid rotation of methyl groups about their CH_3 symmetry axis considerably slows down spin relaxation processes resulting in sharper signals and higher sensitivity, whereby the methyl-TROSY effect offers further improvements especially in large molecular systems.[8-10] Along with advancements in isotope labeling strategies,[11-13] internal motions from picoseconds (ps) to the protein rotational tumbling correlation time, which is typically in the low nanosecond (ns) range, can be probed by ^2H, ^1H, or ^{13}C relaxation experiments. In particular, ^2H-methyl relaxation in proteins was first demonstrated for $^{13}CH_2D$ groups[14, 15] and subsequently extended to $^{13}CHD_2$ moieties,[16, 17] ^1H relaxation was applied to $^{13}CH_2D$ and $^{13}CH_3$ groups in the presence of a highly deuterated protein background,[18-20] ^{13}C transverse relaxation, longitudinal relaxation and the heteronuclear Overhauser enhancement (hetNOE) were determined for $^{13}CH_3$[21, 22] and $^{13}CHD_2$[23] groups, and ^{13}C cross-correlated relaxation was measured for $^{13}CH_3$ groups.[24, 25] On the other hand, slower motions on μs to ms timescales reporting on chemical shift modulations, caused by conformational or chemical exchange, can be measured by $R_{1\rho}$ rotating frame relaxation,[26, 27] Carr-Purcell-Meiboom-Gill (CPMG) relaxation dispersion,[28-31] and chemical exchange saturation

transfer (CEST) experiments[32, 33] on either ^{1}H or ^{13}C spins. However, all these relaxation measurements are insensitive to internal motions on the intermediate ns-μs timescale range, leaving a wide gap in both our knowledge and biological understanding of protein side-chain dynamics (**Figure 1B**).

Other solution NMR parameters and techniques, while important, have not been able to fully remedy this situation. For example, vicinal scalar ^{3}J-couplings[34, 35] and residual dipolar couplings[36] are sensitive to motions from ps to ms timescales, but their interpretation is often complex, since the dynamics is inherently convoluted with effects from the average structure. From a biological point of view, there is no reason to expect that motions on these timescales are absent or are biologically less important than motions observed on other timescales. Methyl-side chain dynamics of proteins can also be probed in the solid state.[37-40] High similarity of longitudinal ^{13}C-methyl relaxation between the solid-state and solution was observed for an SH3 domain after accounting for the effect of rotational tumbling in solution, suggesting a good correspondence of side-chain dynamics in the two states on the low ns and sub-ns timescale.[37]

We recently reported the nanoparticle-assisted NMR spin relaxation (NASR) method for studying protein backbone motions that enable access to ns-μs dynamics to address this well-known blind spot.[41, 42] NASR utilizes non-specific weak interactions between globular proteins and much slower tumbling nanoparticles (NPs) that form a colloidal dispersion at low concentration. The vast majority of protein is in free solution transiently interacting with the nanoparticle surface for only a short fraction of their time. By measuring the ^{15}N transverse relaxation rates of the backbone amide groups in the presence and absence of NPs, the amplitudes of the motions up to rotational tumbling timescales of the NPs (τ_{NP}) can be easily extracted in a structure-independent manner. The NASR method revealed substantial ns-μs dynamics of the functional loops in Im7 and CBD1, while ubiquitin backbone dynamics is largely confined to sub-ns timescales. Here, we introduce NASR to study side-chain dynamics. For this purpose, we use transverse autocorrelated and cross-correlated spin relaxation of methyl groups with their ^{2}H spins or ^{13}C-^{1}H spin pairs as probes. The method is demonstrated for human ubiquitin and colicin E7 immunity protein Im7, which has regions displaying dynamics on the sub-ns and the ns-μs timescale. The results are further corroborated using extended all-atom molecular dynamics simulations.

Materials and Methods

Sample Preparation

For ^{13}C relaxation measurements, uniformly ^{13}C,^{15}N-labeled human ubiquitin and Im7 were expressed and purified as described previously.[41] Fractionally ^{2}H-labeled proteins for ^{2}H relaxation measurements were obtained by growing *E.coli* cells in 99.9% D_2O and using $^{15}NH_4Cl$ and uniformly labeled ^{1}H,^{13}C-glucose as sole nitrogen and carbon sources.[12, 31] This yields approximately equal populations of $^{13}CHD_2$ and $^{13}CH_2D$ methyl-isotopomers with smaller amounts of methyl $^{13}CH_3$ and $^{13}CD_3$ moieties.[12] After His_6-tag cleavage, Im7 protein contains three non-native residues (SNA) at the N-terminus. Ubiquitin was dialyzed into 20 mM sodium phosphate buffer (pH 7.0) and Im7 into 50 mM sodium phosphate buffer (pH 7.0). Both proteins were concentrated to 0.9 to 1.2 mM for NMR measurements.

Levasil CS40-120 (previously known as Bindzil 2040) colloidal anionic silica nanoparticles (SNPs) with average size of 20 nm diameters were obtained from Nouryon™ (previously AkzoNobel) and were characterized previously.[42, 43] Our previously reported TEM data shows a nearly symmetric distribution of the radius of gyration with $\langle R_g \rangle$ = 19.5 +/- 5.3 nm.[43] SNPs were dialyzed into corresponding buffers (20 mM sodium phosphate at pH 7.0 for ubiquitin and 50 mM sodium phosphate at pH 7.0 for Im7) then directly mixed with proteins to prepare the SNP-containing NMR samples. The final SNP concentrations of those samples are in the sub-μM to low μM range. For the samples used in this work, they are 0.1-0.2 μM for ubiquitin and 5-9 μM for Im7. All NMR samples contained 3% D_2O and were stable over the course of the NMR measurements.

NMR Experiments

NMR experiments were performed at 298 K on Bruker AVANCE III spectrometer operating at 850 MHz (19.97 T) equipped with a TCI cryoprobe, except for the ^{2}H relaxation field-dependence measurements on ubiquitin, which were recorded on a Bruker AVANCE III 600 MHz (14.1 T) spectrometer with a TXI cryoprobe. Methyl group resonance assignments were taken from the literature for ubiquitin[17, 44] and for Im7, they were obtained from H(CCO)NH-TOCSY, (H)CC(CO)NH-TOCSY and CT-^{13}C-^{1}H HSQC experiments. The stereospecific

assignments of Val and Leu methyl groups were obtained from CT-^{13}C-^{1}H HSQCs measured on a 10% ^{13}C-labeled sample.[45]

^{2}H relaxation rates $R(D_z)$ (longitudinal relaxation), $R(D_+)$ (transverse relaxation, abbreviated as R_+) and $R(3D_z^2 - 2)$ (quadrupolar order relaxation) were recorded on ^{13}C-^{13}CH$_2$D moieties using established experiments.[14, 15] The recovery delay was set to 2 s and the ^{2}H carrier frequency was placed at the center of the methyl group region at 0.8 ppm. The transverse relaxation rates R_+ were derived from R_1 and $R_{1\rho}$ experiments with ^{2}H spinlock field strength of 1000 Hz and they were converted to R_2 parameters as described in the Supporting Information (SI) in a way that is analogous to the standard ^{15}N relaxation data treatment. The peak intensities were fitted by a mono-exponential decay function $I(t) = I(0) \cdot \exp(-Rt)$ for the extraction of relaxation rate R. Profiles that significantly deviated from the mono-exponential decay behavior and/or with fitting errors larger than 15% were excluded from the analysis.

Methyl group ^{13}C longitudinal R_1 relaxation rates on ^{13}C-^{13}CH$_3$ moieties were collected with a recovery delay of 3 s by the experiment described previously.[21, 25] The ^{13}C-^{1}H dipole-dipole cross-correlation rates Γ were measured according to the experimental scheme by Yang and coworkers[25] with a recovery delay of 2 s. Γ values were extracted from the relative peak intensity profiles using the relationship:

$$\frac{I(\Delta,T)}{I(0,T)} = \cos(\pi J'\Delta) \cdot \frac{3cos(3\pi J_{CH}\Delta)\cdot exp(-4\Gamma T)+(1+x)\cdot cos(\pi J_{CH}\Delta)}{3exp(-4\Gamma T)+(1+x)} \quad (1)$$

where $T = n/J_{CC}$ is the constant time for ^{13}C chemical shifts evolution in the experiments (J_{CC} is the one bond ^{13}C-^{13}C coupling constant). $I(\Delta, T)$ is the peak intensity at delay Δ with constant time T, J_{CH} is the one bond ^{13}C-^{1}H coupling constant, and J' is an additional coupling constant treated here as a free fitting parameter (**Figure S2**). x is a residue specific factor that relates to relaxation during the INEPT transfer and acquisition periods and is treated as an empirical factor that cancels out during the Γ extraction process (**Figure S3**) by collecting two or more experiments with different constant times T (28.5 ms and 57 ms for example) on the same sample (for details, see SI). Leu residues with Cδ and Cγ chemical shift differences that are not much larger than J_{CC} ($|\delta_{C\delta} - \delta_{C\gamma}| < 12\, J_{CC}$) can show significant deviation from **Eq. (1)** due to strong coupling effects between Cδ and Cγ carbons as discussed previously.[25] Methyl groups

L15Cδ1, L43Cδ1 L50Cδ1, L56Cδ1, and L69Cδ1 in ubiquitin, and L3Cδ1, L19Cδ1, L34Cδ2, L37Cδ1, and L38Cδ1 in Im7 met this criterion and were thus excluded from the analysis. M1Cε of Im7 was also excluded, since its profile could not be adequately fit by **Eq. (1).**

The NMR data were processed with NMRPipe[46] and visualized with Sparky.[47] Peak fitting errors were estimated from the differences observed for duplicate delays in the measurements. Error estimates of extracted parameters, including model parameters (see below), were estimated by analytical error propagation or Monte Carlo simulations with 100 or more simulations. The statistical experimental errors were displayed as error bars in the figures.

Model-Free Analysis of Methyl Relaxation

The ^{2}H transverse relaxation rate R_+ of $^{13}CH_2D$ groups is given by:[14, 15, 48, 49]

$$R_+ = \frac{1}{80} \cdot (2\pi \cdot QCC)^2 \cdot [9J_Q(0) + 15J_Q(\omega_D) + 6J_Q(2\omega_D)] \quad (2)$$

where QCC is the quadrupolar coupling constant of 167 kHz when a tetrahedral geometry of the methyl group is assumed (θ_{CD} = 109.5^0).[50] ω_D is the Larmor frequency of ^{2}H and $J_Q(\omega)$ is the spectral density function for quadrupolar relaxation given by **Eq. (4)** (see below).

The ^{13}C-^{1}H methyl cross-correlation rate Γ is given by:[24, 25]

$$\Gamma = \frac{1}{10}\left(\frac{\mu_0}{4\pi}\right)^2\left(\frac{h}{2\pi}\right)^2\gamma_H^2\gamma_C^2 < r_{CH}^{-3} >^2 \cdot \left(4J_{CH,CH}(0) + 3J_{CH,CH}(\omega_C)\right) + \frac{1}{10}\left(\frac{\mu_0}{4\pi}\right)^2\left(\frac{h}{2\pi}\right)^2\gamma_H^4 < r_{HH}^{-3} >^2 \cdot \left(3J_{HH,HH}(\omega_H) + 3J_{HH}(2\omega_H)\right) \quad (3)$$

where μ_0 is the permeability of vacuum, h is the Planck's constant, γ_H and γ_C are the gyromagnetic ratios and ω_H and ω_C are the Larmor frequencies of ^{1}H and ^{13}C. r_{CH} is the C-H bond length in methyl groups and θ_{CH} is the angle between the methyl group C-H bond and the C-C bond rotation axis. These parameters can be set to r_{CH} = 1.135 Å when θ_{CH} = 109.5^0 (tetrahedral geometry, see also **Eq. (4)**) or, alternatively, to r_{CH} = 1.115 Å and θ_{CH} = 110.5^0, whereby the two sets give nearly identical ^{13}C S^2_{axis} values in the model-free analysis.[23] A distance r_{HH} = 1.821 Å between the protons in methyl groups was assumed. $J_{HH}(\omega)$, $J_{CH,CH}(\omega)$ and $J_{HH,HH}(\omega)$ are the autocorrelation and cross-correlation spectral density functions given by **Eqs. (4),(S5)**.

The following extended-model free expression[51, 52] of the spectral density function for methyl groups was used for analysis of the experimental data:[53-55]

$$J_{\mathrm{X}}(\omega) = \frac{1}{9}\cdot S^2_{\mathrm{axis}}\cdot\frac{\tau_{\mathrm{P}}}{1+\omega^2\tau_{\mathrm{P}}^2}+\left(\mathrm{a}_X-\frac{1}{9}\right)\cdot S^2_{\mathrm{axis}}\cdot\frac{\tau_{\mathrm{methyl,eff}}}{1+\omega^2\tau^2_{\mathrm{methyl,eff}}}+\frac{1}{9}\cdot(1-S^2_{\mathrm{axis}})\cdot\frac{\tau_{\mathrm{int,eff}}}{1+\omega^2\tau^2_{\mathrm{int,eff}}}+\left(\mathrm{a}_X-\frac{1}{9}\right)\cdot(1-S^2_{\mathrm{axis}})\cdot\frac{\tau_{\mathrm{eff}}}{1+\omega^2\tau^2_{\mathrm{eff}}} \quad (4)$$

where X stands either for quadrupolar interaction (Q) or dipole-dipole cross-correlated relaxation (CH,CH) with a_Q = 1 and $a_{CH,CH}$ = -1/3. **Eq. (4)** assumes θ_{CD} and θ_{CH} = 109.5^0. S^2_{axis} is the generalized order parameters of the methyl rotation axis. Methyl group rotation around the C-C axis and reorientation of the rotation axis are assumed to be independent, and the protein tumbling is assumed to be isotropic with a rotational correlation time τ_{P}. $\tau^{-1}_{\mathrm{methyl,eff}} = \tau^{-1}_{\mathrm{methyl}} + \tau_{\mathrm{P}}^{-1}$, $\tau^{-1}_{\mathrm{int,eff}} = \tau^{-1}_{\mathrm{int}} + \tau_{\mathrm{P}}^{-1}$, and $\tau^{-1}_{\mathrm{eff}} = \tau^{-1}_{\mathrm{methyl}} + \tau^{-1}_{\mathrm{int}} + \tau_{\mathrm{P}}^{-1}$, where τ_{methyl} is the correlation time of methyl group rotation, usually on the order of tens of ps, and τ_{int} is the correlation time of the reorientation of the rotation axis in a molecular frame. A generalized expression for other autocorrelation and cross-correlation spectral density functions (e.g. $J_{HH,HH}(\omega)$) is given in the SI. All standard methyl group model-free fitting was performed with the above expression except when specifically noted using the LS-2 model described in the SI.

The free protein rotational correlation times τ_{P}, which were extracted from ^{15}N relaxation data measured in the absence of SNPs on the same NMR samples used for the side-chain relaxation measurements, were determined to be 4.1 ns for ubiquitin and 5.3 ns for Im7.

Molecular Dynamics Simulation

Molecular dynamics (MD) simulations of ubiquitin and Im7 were performed using the GROMACS 2020.2 package.[56] The initial structures of ubiquitin and Im7 were built based on crystal structures 1UBQ and 1CEI (PDB codes), respectively. The integration time step was set to 2 fs with all bond lengths containing hydrogen atoms constrained by the LINCS algorithm. A 10 Å cutoff was used for van der Waals and electrostatic interactions. Particle-mesh Ewald summation with a grid spacing of 1.2 Å was used to calculate long-range electrostatic interactions. A cubic simulation box that extends at least 8 Å from the protein surface in every direction was employed, and periodic boundary conditions were applied to all three dimensions. Energy minimization was performed using the steepest descent algorithm for 50,000 steps. The

system was then simulated for 100 ps at constant temperature and constant volume with all protein heavy atoms positionally fixed. Next, the pressure was coupled to 1 atm and the system was simulated for another 100 ps without positional restraints. The final MD production run was performed at constant temperature of 300 K and constant pressure of 1 atm for a total length of 10 μs for ubiquitin and 4 μs for Im7 using the protein force field ff99SBnmr2[57] and the explicit water model TIP3P.[58] Methyl group rotation axis (C-CH_3 bond) NMR S^2_{axis} order parameters were back-calculated from MD trajectories using the isotropic reorientational eigenmode dynamics (iRED)[59] method with averaging time windows of 25 ns and 2 μs.

Results

Methyl Group NASR Measurement Based on ^{2}H Relaxation

^{2}H spin relaxation is dominated by the strong nuclear quadrupolar interaction making ^{2}H spins well-suited as quantitative probes of internal protein dynamics. For proteins with partially deuterated methyl sites, five distinct relaxation rates of a single ^{2}H can be measured on $^{13}CH_2D$ moieties via the well-established experiments by Kay and co-workers,[14, 15] although a subset of three experiments is sufficient for the unambiguous determination of the three spectral densities $J(0), J(\omega_{\mathrm{D}}), \mathrm{and}\, J(2\omega_{\mathrm{D}})$ at a given magnetic B_0-field. Motional parameters that describe the internal dynamics of each methyl group, namely the internal correlation times τ_{methyl} of the rotation about the 3-fold symmetry axis, the correlation time τ_{int} of the reorientation of the methyl symmetry axis defined by the C-CH_3 bond vector, and the generalized order parameter of the rotation axis S^2_{axis}, can then be extracted by standard model-free analysis.[17, 53]

Here, we focus on the three ^{2}H relaxation rates that belong to longitudinal magnetization $R(D_{\mathrm{z}})$, in-phase transverse magnetization $R(D_+)$ (abbreviated below as R_+), and quadrupolar order $R(3D_{\mathrm{z}}^2 - 2)$ in the presence and absence of nanoparticles. Among them, the transverse relaxation rate R_+ is the relaxation parameter that is by far most sensitive to the presence of NPs as manifested by an elevation of R_+^{NP} due to transient interactions between the proteins and the slowly tumbling NPs (**Figure 1A**). Analogous to the NASR measurement of ^{15}N transverse relaxation R_2, R_+^{NP}can be expressed as:[41]

$$R_+^{\mathrm{NP}} = p_{\mathrm{b}} \cdot R_+^{\mathrm{bound}} + (1 - p_{\mathrm{b}}) \cdot R_+^{\mathrm{free}} \quad (5)$$

where R_+^{bound} and R_+^{free} are the R_+ relaxation rates of proteins bound to NPs and in free solution, respectively, and p_b is the population of protein bound to NPs. The increase in R_+ upon the addition of NPs is then give by:

$$\Delta R_+ = R_+^{\mathrm{NP}} - R_+^{\mathrm{free}} \propto \tau_{\mathrm{NP}} \cdot p_\mathrm{b} \cdot S_{\mathrm{axis}}^2 \quad (6)$$

where τ_{NP} is the rotational tumbling correlation time of NPs and S_{axis}^2 is the same as in **Eq. (4)**. **Eq. (6)** is valid under conditions described previously,[60] including $\tau_{\mathrm{methyl}}, \tau_{\mathrm{int}} < \tau_{\mathrm{NP}}/10$. Depending on NP size, τ_{NP} is usually on the order of hundreds of ns to tens of μs. Since τ_{methyl} is in the ps range, all methyl groups fulfill the above condition for τ_{methyl}. The global factor $\tau_{\mathrm{NP}} \cdot p_\mathrm{b}$ depends on the NP concentration and, for a given NP-protein sample, it is the same for all methyl groups in the protein. Importantly, S_{axis}^2 derived from ΔR_+, in the following denoted as $S_{\mathrm{axis}}^2(\Delta R_+)$, reports on all internal motions covering the full range from ps to τ_{NP} timescales or ps to μs. This is in contrast to the traditional model-free parameter S_{axis}^2(MF), which can be derived from relaxation data in the absence of NPs, as it is only sensitive to internal motions that are faster than the protein rotational tumbling correlation time τ_P, i.e. on ps to low-ns timescales. Hence, the NASR ^{2}H-ΔR_+ parameters report on motions exceeding the accessible timescales of the traditional model-free analysis by 2-3 orders of magnitudes (**Figure 1B**). This timescale window is similar to that probed by backbone ^{15}N-ΔR_2 NASR.[41]

The ^{2}H-ΔR_+-based NASR method is experimentally demonstrated for methyl-bearing side chains of the two globular proteins ubiquitin and Im7. The ^{2}H R_+ rates were collected in the presence and absence of 20 nm diameter anionic silica nanoparticles (SNPs). For comparison, S_{axis}^2(MF) were derived from experimental R_+, $R(D_\mathrm{z})$ and $R(3D_\mathrm{z}^2 - 2)$ relaxation rates of the free protein, which were subsequently used as benchmarks for the total amount of sub-ns dynamics. For ubiquitin, S_{axis}^2(MF) values were determined by simultaneously fitting the results of measurements performed at 600 MHz and 850 MHz NMR fields. The resulting S_{axis}^2(MF) values were found to be consistent with the ones reported previously in the literature.[17, 22] The Im7 data were collected at a single magnetic field strength of 850 MHz ^{1}H frequency.

The ubiquitin ^{2}H-ΔR_+ rates obtained at 850 MHz display a strikingly linear dependence on S_{axis}^2(MF) values with a high Pearson correlation coefficient (R) of 0.971 (**Figure 2A**). Because ΔR_+ and the corresponding order parameter $S_{\mathrm{axis}}^2(\Delta R_+)$ are sensitive to motions on a

much broader timescale range than $S^2_{\mathrm{axis}}(\mathrm{MF})$, it is expected that in general $S^2_{\mathrm{axis}}(\Delta R_+) \leq S^2_{\mathrm{axis}}(\mathrm{MF})$, so that:

$$\Delta R_+ \propto S^2_{\mathrm{axis}}(\Delta R_+) \leq S^2_{\mathrm{axis}}(\mathrm{MF}) \tag{7}$$

Therefore, a global linear correlation between ΔR_+ and $S^2_{\mathrm{axis}}(\mathrm{MF})$ is only predicted when the internal motions of all methyl groups measured are confined to the ps to low-ns timescales. On the other hand, methyl groups with dynamics on slower timescales that exceed τ_{P} will result in a site-specific reduction of ΔR_+ rates, thereby deviating from the linear relationship with the $S^2_{\mathrm{axis}}(\mathrm{MF})$ values. The linear agreement between the ΔR_+ and $S^2_{\mathrm{axis}}(\mathrm{MF})$ values observed for ubiquitin suggests that under the sample conditions used in this work there are no significant amounts of slower ns-µs timescale motions present for these methyl groups. Of note, the ΔR_+values obtained at 600 MHz are nearly identical to those at 850 MHz (**Figure S1**), which is entirely consistent with the field-independent nature of the quadrupolar coupling constant as prefactor of the dominant spectral density *J*(0) term.

For Im7, the ^{2}H-ΔR_+ rates vs. $S^2_{\mathrm{axis}}(\mathrm{MF})$ correlation plot shows a different behavior than that observed for ubiquitin (**Figure 2B**). It reveals that the methyl groups are clustered into two groups: one follows a linear behavior as for ubiquitin, whereas for the other group the ΔR_+ values lie systematically below the linear regression line. These smaller ΔR_+ values hint at the presence of slower dynamics for the methyl groups in this cluster in accordance with **Eq. (7)**. This cluster consists of the methyl groups that reside in or near loop I in Im7, which is the loop previously observed to exhibit ns-µs backbone dynamics from NASR ^{15}N-ΔR_2 analysis.[41]

For both ubiquitin and Im7 it is found that the ΔR_+ rates have a positive intercept compared to S^2_{axis}, i.e. $\Delta R_+ > 0$ even when S^2_{axis} approaches zero (**Figure 2A,B**). This offset is not included in **Eq. (6)** and it is not limited to methyl groups with low S^2_{axis} values as it is uniformly present throughout the entire range of $S^2_{\mathrm{axis}}(\mathrm{MF})$ values. The offset can be determined by a linear regression between ΔR_+ and S^2_{axis} following $\Delta R_+ = A \cdot S^2_{\mathrm{axis}} + B$, which yields the slope *A* and offset (intercept) *B*, when including only residues *without* slow motions. This class of residues can be determined by cluster analysis using the DBSCAN[61] algorithm as demonstrated in **Figure S7**. Next, S^2_{axis} is determined for residues *with* ns–µs dynamics using the relationship $S^2_{\mathrm{axis}}(\Delta R_+) = (\Delta R_+ - B)/A$. In this way, quantitative dynamic information can be

extracted for residues exhibiting slower ns-μs dynamics after they have been identified based on their positions below the linear regression line.

^{13}C Cross-Correlation as an Alternative Probe

As an alternative to ^{2}H spin relaxation experiments, methyl group dynamics can also be probed by ^{13}C relaxation. The transverse relaxation rates ^{13}C-R_2 are usually measured in ^{12}C-$^{13}CHD_2$ methyl moieties to minimize multi-exponential relaxation decays caused by ^{13}C-^{13}C dipolar couplings and dipole-dipole cross correlation effects,[23] thereby necessitating a specifically ^{13}C, ^{2}H-labeled sample. Recent progress allowed measurements of ^{13}C-^{1}H dipole-dipole cross-correlated cross-relaxation rates Γ directly for uniformly ^{13}C-labeled and fully protonated samples (^{13}C-$^{13}CH_3$).[25] ^{13}C cross-correlation Γ is immune to the external protons and the conformational exchange on the chemical shift timescale (~ms), which simplified interpretation of such data. Likewise to autocorrelated transverse relaxation, Γ is dominated by the spectral density at near zero-frequency $J(0)$, which makes it highly sensitive to the binding of proteins to the NP surface. Analogous to ^{2}H-ΔR_+, the increase in the cross-correlation rates Γ in the presence of NPs can then be expressed as:

$$\Delta\Gamma = \Gamma^{\mathrm{NP}} - \Gamma^{\mathrm{free}} \propto \tau_{\mathrm{NP}} \cdot p_{\mathrm{b}} \cdot S^2_{\mathrm{axis}} \tag{8}$$

which holds for $\tau_{\mathrm{int}} < \tau_{\mathrm{NP}}/10$. ΔΓ is linearly correlated with the order parameter S^2_{axis} by the global factor $\tau_{\mathrm{NP}} \cdot p_{\mathrm{b}}$, and the ΔΓ-derived $S^2_{\mathrm{axis}}(\Delta\Gamma)$ is sensitive to internal motions on ps to sub-τ_{NP} timescales in line with ^{2}H-ΔR_+ fulfilling also the inequality $\Delta\Gamma \propto S^2_{\mathrm{axis}}(\Delta\Gamma) \leq S^2_{\mathrm{axis}}(\mathrm{MF})$, which is analogous to that for ΔR_+ discussed in the previous section.

We measured ^{13}C-Γ in the presence and absence of the 20 nm anionic SNPs for ubiquitin and Im7 under identical experimental conditions (pH 7 and 298 K) as for ^{2}H-ΔR_+ data collection. The correlation plots of the ^{13}C-ΔΓ rates against the traditional model-free order parameters $S^2_{\mathrm{axis}}(\mathrm{MF})$ derived from ^{2}H relaxation are depicted in **Figure 2C,D**. ΔΓ of ubiquitin has a pronounced linear relationship to $S^2_{\mathrm{axis}}(\mathrm{MF})$. By contrast, for Im7 the methyl groups are split into two distinct clusters, where one follows a linear regression line and the other cluster has its ΔΓ values below the regression line. The methyl groups following the linear regression have most of their internal motions already sampled on the sub-ns timescale, since these are the motions

captured also by $S^2_{\text{axis}}(\text{MF})$ (plotted along x-axis). The methyl groups in the other cluster with the lower ΔΓ values experience the presence of additional motions on the slower ns-μs timescale. The methyl groups of the 2nd cluster are localized in or near loop I, in agreement with the behavior observed for ΔR_+ when also compared with $S^2_{\text{axis}}(\text{MF})$. As for the ΔR_+ rates, ΔΓ approaches a finite offset when S^2_{axis} approaches 0. Likewise to the conversion of ΔR_+ to $S^2_{\text{axis}}(\Delta R_+)$ described above, the conversion of ΔΓ to $S^2_{\text{axis}}(\Delta\Gamma)$ follows two steps: (i) identification of the outliers with slow dynamics from the ΔΓ vs. $S^2_{\text{axis}}(\text{MF})$ correlation plot; (ii) determination of the linear regression parameters A' and B' from ΔΓ vs. $S^2_{\text{axis}}(\text{MF})$ after excluding the outliers leading to $\Delta\Gamma = A' \cdot S^2_{\text{axis}}(\Delta\Gamma) + B'$ from which $S^2_{\text{axis}}(\Delta\Gamma)$ can be determined for any experimentally determined ΔΓ value.

From the measurements of the free sample, the cross-correlation rate Γ together with the ^{13}C longitudinal relaxation rate R_1 allows determination of model-free order parameters $S^2_{\text{axis}}(\text{MF})$ using the LS-2 model.[25] These ^{13}C-relaxation derived $S^2_{\text{axis}}(\text{MF}, ^{13}\text{C})$ values are strongly correlated with the ^{2}H relaxation derived $S^2_{\text{axis}}(\text{MF}, ^2\text{H})$ values (LS-2 analysis), except that they are systematically elevated by < 0.1. This permits direct extraction of motional information contained in ΔΓ from the ΔΓ vs. $S^2_{\text{axis}}(\text{MF}, ^{13}\text{C})$ correlation plots (**Figure S4**), which hold the same conclusions as **Figure 2C,D**. Therefore, the ΔΓ-based NASR analysis can be reliably and independently performed solely with a uniformly ^{13}C labeled samples without the need for ^{2}H labeling by measuring the two relaxation rates R_1 and Γ in the absence of NPs and the Γ rates in the presence of NPs. It considerably simplifies sample preparation making NASR of methyl-side chains more easily applicable to a wide range of protein systems.

Methyl Group Dynamics in Ubiquitin

Figure 3A shows the comparison between the axial order parameter derived from ^{2}H and ^{13}C based NASR measurements $S^2_{\text{axis}}(\Delta\text{R}_+)$ and $S^2_{\text{axis}}(\Delta\Gamma)$, and the standard model-free order parameters $S^2_{\text{axis}}(\text{MF})$ of ^{2}H relaxation data. The $S^2_{\text{axis}}(\Delta\text{R}_+)$ and $S^2_{\text{axis}}(\Delta\Gamma)$ values obtained from independent measurements on two different types of spins experiencing quadrupolar vs. dipolar spin relaxation mechanisms are highly consistent with each other and they both agree remarkably well with $S^2_{\text{axis}}(\text{MF})$ successfully reproducing even the fine zig-zag pattern (**Figure 3A**). This agreement indicates that among the ps to low-μs timescale probed here, the methyl group

dynamics in ubiquitin is largely confined to the ps to low-ns regime. It mirrors our previous observation for the ubiquitin backbone dynamics, which also lack ns-μs motions according to ^{15}N-ΔR_2 NASR measurements.[42] The average of $S^2_{\text{axis}}(\Delta R_+)$ and $S^2_{\text{axis}}(\Delta\Gamma)$ values, termed S^2_{axis}(NASR), were then mapped onto the ubiquitin crystal structure in **Figure 3D**. Unlike the backbone order-parameters, where high S^2 values are generally expected for the residues in rigid secondary structures, the methyl group S^2_{axis} are semi-quantitatively related to the solvent accessibility, the number of torsion angles between the backbone and the methyl group and the local contacts between the methyl group with its surroundings.[62]

All-atom molecular dynamics (MD) simulations can provide an independent *in silico* view of methyl group dynamics. A 10-μs MD trajectory of ubiquitin was performed in explicit water solvent with our recently developed ff99SBnmr2 protein force field.[57] The methyl group axial order parameters were then computed from the trajectory using the isotropic reorientational eigenmode dynamics (iRED) method with time-averaging windows τ_{iRED}= 25 ns and 2 μs. τ_{iRED}= 25 ns (~5τ_{P}) corresponds to the fast motions accessible by the traditional model-free analysis,[59] whereas τ_{iRED}= 2 μs captures also motions on the slow timescales accessible by NASR. The S^2_{axis}(MD) are found to show limited decrease when increasing the τ_{iRED} window from 25 ns to 2 μs (**Figure 3B**). In addition, both S^2_{axis}(NASR) and S^2_{axis}(MF) are largely consistent with the S^2_{axis}(MD) values with correlation coefficients of 0.93 and 0.88 (**Table S3**). It further corroborates the conclusion about the absence of significant amounts of slow ns-μs motions in the methyl-side chains of ubiquitin.

The internal dynamics of ubiquitin in solution, both for backbone and side-chain methyl groups, have been the subject of extensive NMR studies in the past. Side-chain rotamer populations were derived from the ^{3}J$_{\text{N-C}\gamma}$ and ^{3}J$_{\text{C'-C}\gamma}$ scalar J-couplings ($S^2_{\text{axis}}(J)$) or from the rotamer ensembles determined by residual dipolar couplings in two alignment media ($S^2_{\text{axis}}(D)$) and translated to order-parameters at Cγ positions of Val, Ile and Thr residues.[34] The rotameric distribution-derived order parameters are sensitive to motions up to ms timescales, i.e. even broader than those accessible by NASR. However, both $S^2_{\text{axis}}(J)$ and $S^2_{\text{axis}}(D)$ can be ill-determined, which may cause different results by the two approaches. With the exception of methyl sites where $S^2_{\text{axis}}(J)$ and $S^2_{\text{axis}}(D)$ show large discrepancies, the $S^2_{\text{axis}}(J)$ and $S^2_{\text{axis}}(D)$

values largely agree with $S^2_{\mathrm{axis}}(\mathrm{NASR})$ (**Figure 3C**). Although some methyl groups display lower $S^2_{\mathrm{axis}}(J)$ or $S^2_{\mathrm{axis}}(D)$ values than $S^2_{\mathrm{axis}}(\mathrm{NASR})$, $S^2_{\mathrm{axis}}(\mathrm{NASR})$ is usually within the sizeable uncertainty intervals of $S^2_{\mathrm{axis}}(J)$ and $S^2_{\mathrm{axis}}(D)$.

Methyl Group Dynamics in Im7

The ^{2}H-based $S^2_{\mathrm{axis}}(\Delta\mathrm{R}_+)$ and ^{13}C-based $S^2_{\mathrm{axis}}(\Delta\Gamma)$ profiles of the methyl groups of Im7 are highly consistent with each other with both showing the presence of intermediate ns-μs dynamics around the loop I region of Im7 (**Figure 4A**). The motional amplitudes of the loop I residues as reflected by their S^2_{axis} values derived from the independent ^{2}H and ^{13}C relaxation measurements are extremely similar to each other, but they are much lower than $S^2_{\mathrm{axis}}(\mathrm{MF})$. This suggests the existence of additional slower timescale motions in these side chains that are missed by traditional $S^2_{\mathrm{axis}}(\mathrm{MF})$ analysis. On the other hand, for other residues of Im7 not belonging to loop I, $S^2_{\mathrm{axis}}(\Delta\mathrm{R}_+)$ and $S^2_{\mathrm{axis}}(\Delta\Gamma)$ show good consistency with $S^2_{\mathrm{axis}}(\mathrm{MF})$. For Ala residues, the vicinity of the methyl rotation axes (Cα-Cβ bond vectors) to the backbone suggests they experience overall similar amounts of motion as the corresponding backbone N-H vectors. Residues Ala13, Ala77, and Ala78 of Im7, which are located in helix I and helix IV, were identified to have their backbone motions confined to the sub-ns timescale regime according to NASR ^{15}N-ΔR_2. The consistency between $S^2_{\mathrm{axis}}(\Delta\mathrm{R}_+)$, $S^2_{\mathrm{axis}}(\Delta\Gamma)$ and $S^2_{\mathrm{axis}}(\mathrm{MF})$ of these alanine methyl groups with their backbone dynamics are in further support of the NASR results.

The methyl group axial order parameters were back-calculated from a 4-μs MD trajectory of Im7 analogous to the approach used for ubiquitin. When increasing the τ_{iRED} window from 25 ns to 2 μs, the $S^2_{\mathrm{axis}}(\mathrm{MD})$ show an additional decrease that is by far the largest in loop I (**Figure 4B**). This is in near-quantitative agreement with the experimentally observed difference between $S^2_{\mathrm{axis}}(\mathrm{NASR})$ and $S^2_{\mathrm{axis}}(\mathrm{MF})$ for this region reflecting slower loop motions. The global correlation coefficients of $S^2_{\mathrm{axis}}(\mathrm{MD})$ with $S^2_{\mathrm{axis}}(\mathrm{NASR})$ and $S^2_{\mathrm{axis}}(\mathrm{MF})$ are 0.88 and 0.89, respectively (**Table S3**). Like for ubiquitin, these correlation coefficients are notably high for methyl-side chains considering that the MD trajectories were not subjected to any form of *a posteriori* treatment, such as reweighting or fitting, for the purpose of improving the agreement with experiment. Taken together, the MD simulation correctly reproduces the enhanced slow

dynamics in loop I observed by NASR and elsewhere it displays semi-quantitative to quantitative agreement with experiment.

Discussion

Six of the 20 naturally occurring amino acids contain one or multiple methyl groups. Because they are often distributed across many different protein parts, as illustrated for ubiquitin and Im7 in **Figures 3D**,**4C**, they serve as useful site-specific structural and dynamics probes in functional protein studies in solution. Although NMR methods are able to probe motions over a wide spectrum of timescales, the paucity of information about ns–μs motions using existing methods has led to a notable gap in knowledge, which nanoparticle-assisted spin relaxation (NASR) promises to overcome. It has been demonstrated here how the backbone NASR ^{15}N-ΔR_2 approach can be extended to methyl groups to quantitatively monitor dynamics of side chains by measuring differential $^{13}CH_2D$ ^{2}H-ΔR_+ or $^{13}CH_3$ ^{13}C-$\Delta\Gamma$ relaxation in the presence and absence of anionic silica nanoparticles. The resulting experimental S^2_{axis}(NASR) profiles quantitatively report about internal dynamics on the ps to τ_{NP} (low-μs) timescale thereby closing the observation gap of protein dynamics by existing methods. In tandem with the standard model-free analysis, NASR is able to pinpoint the presence and absence of ns to low-μs motions as demonstrated here for ubiquitin and Im7. Although the correlation times associated with S^2_{axis}(NASR) cover a much broader timescale regime than traditional NMR spin relaxation, for a given methyl group their precise value(s) are not specified. By repeating NASR experiments with nanoparticles of different size, and hence different τ_{NP}, it may be possible to obtain such site-specific correlation time information.

Human ubiquitin has served as a model system to study protein structure and function by new NMR methods. Ubiquitin is thermodynamically unusually stable[63] and its amino-acid sequence is highly conserved across different eukaryotic species.[64] A recent backbone NASR ^{15}N-ΔR_2 study showed that on ns–μs timescales ubiquitin is dynamically notably "silent".[42] On sub-ns timescales, on the other hand, ubiquitin displays characteristic internal dynamics, especially in the loop region of the N-terminal β-hairpin and the disordered C-terminal tail.[65-67] On even slower timescales (> 10 μs) than those accessible by NASR, ubiquitin is known to

undergo additional conformational exchange involving a flip of peptide bond D52-G53 as identified by relaxation dispersion experiments.[68] Our NASR methyl results show a large variety of dynamics behavior among residues ranging from nearly static ($S^2 > 0.9$) to highly dynamic ($S^2 < 0.2$) (**Figure 3**). The most dynamic residues are Leu8, which is in the loop of the N-terminal β-hairpin, Ile44 at the end of β-strand III, and Val70, Leu71, Leu73 in the C-terminal tail. Common to all side-chain methyl moieties is that their dynamics amplitudes are essentially unaltered between a standard MF analysis and NASR, as is reflected in the high correlation of $^{13}CH_2D$ ^{2}H-ΔR_+, $^{13}CH_3$ ^{13}C-$\Delta\Gamma$ relaxation and S^2_{axis}(MF) (**Figure 2A,C**). It suggests that dominant side-chain motions occur predominantly on fast sub-ns timescales whereas slower ns–μs timescale motions are essentially absent. This leads to the view that ubiquitin is a protein that samples its dominant conformational substates almost exclusively on fast sub-ns timescales both for the backbone and its methyl-bearing side chains. These findings are further corroborated by a 10 μs MD trajectory of ubiquitin in explicit solvent, which reaches convergence of both backbone and side-chain motions on the low ns timescale with its computed methyl order parameters in good agreement with both NASR and MF. The agreement between NASR and MF analysis also indicates that ubiquitin-SNP interactions do not noticeably alter its internal dynamics. In a recent ^{13}C-high-resolution relaxometry study the dynamics at Ile Cδ1 positions in ubiquitin were determined over B_0 fields ranging from 0.33 to 22.3 T.[69] This approach allows the determination of the internal correlation time distribution from the ps into the low-ns range with higher accuracy compared to standard MF.[69, 70] From the seven Ile residues, the relaxometry data identified three methyl groups (Ile13, Ile36 and Ile44) with well-defined ns motions whereby the S^2_{axis} values derived from relaxometry are systematically lower than the corresponding S^2_{axis}(MF) values by a modest amount (<0.1). The relaxometry S^2_{axis} values agree very well with S^2_{axis}(NASR) for Ile13 and Ile 44 and show a small difference (<0.1) for Ile36 (**Figure S5**). The S^2_{axis}(NASR) values also correlate remarkably well with methyl order parameters reported in a solid-state NMR study of ubiquitin obtained from REDOR-derived ^{13}C-^{1}H dipolar coupling measurements[71] with a Pearson correlation coefficient R of 0.93 for 27 methyl groups comprising Val, Leu and Ile residues that were characterized by both methods (the slope is however not unity, an artifact that was presumably caused by radio-frequency field calibration in the solid-state experiments as discussed elsewhere[72]). Since solid-state dipolar couplings are

sensitive to dynamics from ps to μs, the high correlation with NASR suggests that the methyl-bearing side chains of ubiquitin in both the crystalline state and in solution experience very similar cumulative effects of dynamics over this broad range of timescales, whereby the dominant motional processes take place on the low ns to sub-ns timescale as discussed above.

The biological role of the four-helix bundle protein Im7 is to specifically recognize and tightly bind to the endonuclease domain of the bacterial toxin colicin E7 with binding affinity in the fM-pM range to inactivate E7 and neutralize its toxicity.[73, 74] Loop I of Im7 (Val27 to Asp31) plays a dominant role in these interactions as the side-chains of Asp31 and Asp35 form strong and highly specific salt bridges with basic residues (Arg520, Lys525, and Lys528) of the endonuclease domain of colicin, which are supplemented by several direct or water-mediated hydrogen bonds between residues of the two proteins.[73] Previous backbone NASR ^{15}N-ΔR_2 data revealed that loop I of free Im7 samples a wide range of conformations on ns-μs timescales, which is accompanied by fraying motions of the C-terminus of the first α-helix adjacent to loop I. The ns-μs backbone motions of loop I is expected to be accompanied by reorientations of the side-chain methyl groups on similar timescales, which is consistent with the slow ns-μs motions of the methyl groups observed here in or near loop I, including residues Val27, Ala28, Ala29, Thr30 and Val33, as identified by the NASR ^{2}H-ΔR_+ and ^{13}C-ΔΓ measurements reported in this work (**Figures 2B,2D,4A**). It shows that the high level of flexibility on slow timescales of loop I extend into its side chains. Although the methyl-bearing side chains measured here are not part of the salt bridges themselves, their adjacent locations suggest that Asp31 and Asp35 experience similar types of large amplitude, slow-timescale motions prior to binding to E7. Such pronounced plasticity of this region in free Im7 is likely to enable the fine-tuning and optimization of these attractive electrostatic interactions between Im7 and E7 contributing to their unusually strong binding affinity. It should be noted that in addition Im7 exhibits slow ms motions reflecting unfolding dynamics of helix III as observed by Carr-Purcell-Meiboom-Gill (CPMG) relaxation dispersion experiments.[31, 75] These motions appear to be unrelated to the ns - μs motions in loop I reported here by NASR.

According to **Eqs. (6),(8)**, the magnitude of NASR effects depends both on the size of the nanoparticles via τ_{NP} and the bound protein population p_b. For the 20 nm diameters NPs (τ_{NP} = 0.91 μs), p_b is estimated to be of the order of 1% to achieve an optimal NASR effect. In addition,

it also depends on the rate of exchange k_{ex} of the protein–nanoparticle binding process as has been recently discussed theoretically by solving a stochastic Liouville equation (SLE).[60] In order that the NASR effect is experimentally observable, as is the case in this work for ^{15}N-ΔR_2, ^{2}H-ΔR_+ and ^{13}C-$\Delta\Gamma$, k_{ex} needs to be slow compared to the free protein rotational tumbling rate ($k_{ex} < 1/\tau_P$<10^7-10^8 s^{-1}), but fast compared to differences of transverse relaxation rates of free and bound states (k_{ex} >10^2-10^3 s^{-1}). The systematic offset observed when plotting differential NASR rates vs. S^2_{axis} correlation does not seem to be caused by specific protein interactions with SNPs that cause rigidification of methyl-side chains, i.e. an increase of ΔR_+, in a residue-specific manner for methyl groups that directly interact with the SNP surface. For example, solvent-exposed methyl groups in protein regions with positively charged surface patches, which interact most strongly with the anionic SNPs, would be expected to be most susceptible to such effects, but this is not observed here. The offset is also not the result of a change in the viscosity of the protein sample caused by the presence of SNPs. The low SNP concentration hardly affects the overall viscosity of the NMR sample, which is confirmed, e.g., by the indifference of the longitudinal relaxation rates ^{2}H $R(D_z)$, $R(3D_z^2 - 2)$, and ^{15}N-R_1 on the presence of SNPs. The offset is B_0-field independent as it remains the same for measurements at 600 MHz and 850 MHz proton frequency. The offset also seems not to be caused by paramagnetic relaxation contributions as it not enhanced for nuclei with a larger γ. It is possible that this effect is a consequence of additional fast exchange processes present, such as transient encounters between the protein molecules and the SNPs. Such effects are not captured by **Eqs. (5),(6),(8)** that assume a simple 2-site exchange process and may require a mathematically more rigorous but computationally expensive treatment based on the stochastic Liouville equation (SLE). The NASR rescaling approach described here works particularly well when a sufficient number of protein sites exist whose dynamics lie predominantly in the sub-ns range serving as reference. Future NASR studies with different types of nanoparticles should shed more light on the origin of the offset effect. It should be noted that for backbone ^{15}N-NASR we have not found any evidence for the presence of an offset effect for the same proteins studied here. If present, it would need to be significantly smaller than that observed for methyl groups.

NASR with ^{2}H nuclei has pros and cons. On the one hand, the strong ^{2}H quadrupolar relaxation mechanism makes dipolar relaxation contributions from auto- and cross-correlation terms negligible,[15, 76] thus providing the experimental isolation of this relaxation mechanism and

allowing the robust extraction of dynamics parameters. On the other hand, quadrupolar relaxation causes the rapid loss of magnetization during the experiments leading to decreased sensitivity (signal-to-noise) of the spectra, especially for the NP-containing samples. For comparison, the NP-containing sample requires about twice the measurement time of the NP-free sample to achieve on average a similar signal-to-noise ratio. When random ^{2}H-labeling is used, as in this work, it yields $^{13}CH_2D$ isotopomers with less than 50% abundance for each methyl site,[12] thereby further reducing the sensitivity. The latter issue can be addressed for Ile, Leu, Val residues by using specifically labeled precursors during protein expression.[11] Still, magnetization loss due to relaxation makes the application of NASR ^{2}H-ΔR_+ measurements to large protein systems more challenging. On the other hand, the ^{13}C cross-correlation Γ measurement has better sensitivity with peak-intensity errors usually within 1% for the measurements we performed here, even for the SNP-containing samples. Although extraction of the Γ rates is more complicated compared to the mono-exponential fitting of ^{2}H relaxation, the ^{13}C-ΔΓ measurement has the advantage that no specific ^{2}H labeling is required and it opens up the possibility to study NASR-based methyl dynamics on large protein systems and their complexes.

In addition to a direct mechanistic and site-specific interpretation of methyl-side chain S^2 order parameters, they can also be used as localized probes to measure the protein conformational entropy.[77-79] Changes of side-chain order parameters upon protein-ligand interactions can provide important insights about the underlying thermodynamic driving forces. Ideally, S^2 order parameters interpreted in this way should reflect motions on all timescales that are biologically relevant. By greatly extending the range of timescales observable by NMR spin relaxation, NASR S^2 values should help improve the accuracy of conformational entropy estimations of protein-ligand interaction studies and further highlight the role of entropy in protein function.

Another potentially useful application of NASR concerns the validation of molecular dynamics (MD) computer simulations. As continuous progress in MD now allows the routine simulation of trajectories of proteins into the μs range,[80] the assessment of the accuracy of such simulations is a major challenge. The main reason is that quantitative experimental information about (sub-)μs protein dynamics with site-specific resolution remains notably sparse. In the case of methyl-side chains, their quantitative modeling has been more difficult than the backbone,

although important progress has been made in recent years.[54, 81-84] NASR S^2 order parameters will provide new important quantitative benchmarks allowing an independent evaluation of the accuracy of long μs MD trajectories at many different protein sites. Such information should also prove useful for guiding the improvement of current MD force fields.

Conclusion

In the past, the quantitative experimental characterization of protein side-chain motions on intermediate nanosecond to microsecond timescales has largely remained elusive. This situation is addressed here by the introduction of nanoparticle-assisted spin relaxation for methyl-bearing amino acids. Transverse autorelaxation of partially deuterated CH_2D groups and cross-correlated spin relaxation of uniformly $^{13}CH_3$-labeled methyl moieties produce highly consistent $S^2_{\mathrm{axis}}(\mathrm{NASR})$ profiles for both ubiquitin and Im7. It demonstrates the robustness of the methyl-NASR method to extract quantitative information about protein side-chain dynamics on an exceptionally wide ps-μs timescale range that covers also many biologically relevant dynamics events as evidenced for loop I motions of Im7. Since methyl groups are often found in hydrophobic protein cores and functional binding interfaces, the relatively easy experimental accessibility of $S^2_{\mathrm{axis}}(\mathrm{NASR})$ parameters can provide novel and more comprehensive insights about the role of methyl-bearing side chains and their surrounding for protein stability, protein-protein and protein-ligand interactions that are pertinent to their biological function.

Supporting Information

Theoretical basis for extraction of Γ values, model-free analysis, Stokes-Einstein-Debye relationship; Tables with relaxation rates of ubiquitin and Im7 and quantitative comparison between experimental and MD-derived S^2_{axis} values; Figures with NMR-field dependence of NASR, representative intensity profiles of ^{13}C-Γ cross-correlation rates and their extraction as a function of T, comparison between S^2_{axis} values determined by different method, MD-derived S^2_{axis} as a function of averaging window, cluster analysis for identification of side-chains with slow dynamics. This material is available free of charge via the Internet at http://pubs.acs.org.

Acknowledgements

We thank Dr. Daiwen Yang for the ^{13}C cross-correlated relaxation NMR pulse sequence and discussion about relaxation rate extraction, Dr. Frans Mulder for providing the ^{2}H relaxation NMR pulse sequences, and Ms. Stacey Wardenfelt for her help in protein purification. This work was supported by the U.S. National Science Foundation (grant no. MCB-1715505). All NMR experiments were performed at the CCIC NMR facility at The Ohio State University. The MD simulations were performed at the Ohio Supercomputer Center.

References

1. Kovermann, M.; Rogne, P.; Wolf-Watz, M., Protein dynamics and function from solution state NMR spectroscopy. *Q. Rev. Biophys.* **2016,** *49*, e6.
2. Choy, W.-Y.; Shortle, D.; Kay, L. E., Side chain dynamics in unfolded protein states: an NMR based 2H spin relaxation study of Δ131Δ. *J. Am. Chem. Soc.* **2003,** *125* (7), 1748-1758.
3. Kim, J.; Ahuja, L. G.; Chao, F.-A.; Xia, Y.; McClendon, C. L.; Kornev, A. P.; Taylor, S. S.; Veglia, G., A dynamic hydrophobic core orchestrates allostery in protein kinases. *Sci. Adv.* **2017,** *3* (4), e1600663.
4. Lee, A. L.; Kinnear, S. A.; Wand, A. J., Redistribution and loss of side chain entropy upon formation of a calmodulin–peptide complex. *Nat. Struct. Biol.* **2000,** *7* (1), 72-77.
5. Tzeng, S.-R.; Kalodimos, C. G., Protein activity regulation by conformational entropy. *Nature* **2012,** *488* (7410), 236-240.
6. Verteramo, M. L.; Stenström, O.; Ignjatović, M. M.; Caldararu, O.; Olsson, M. A.; Manzoni, F.; Leffler, H.; Oksanen, E.; Logan, D. T.; Nilsson, U. J.; Ryde, U.; Akke, M., Interplay between conformational entropy and solvation entropy in protein–ligand binding. *J. Am. Chem. Soc.* **2019,** *141* (5), 2012-2026.
7. Palmer III, A. G., NMR characterization of the dynamics of biomacromolecules. *Chem. Rev.* **2004,** *104* (8), 3623-3640.
8. Ruschak, A. M.; Kay, L. E., Methyl groups as probes of supra-molecular structure, dynamics and function. *J. Biomol. NMR* **2010,** *46* (1), 75.
9. Rosenzweig, R.; Kay, L. E., Bringing dynamic molecular machines into focus by methyl-TROSY NMR. *Annu. Rev. Biochem.* **2014,** *83*, 291-315.
10. Boswell, Z. K.; Latham, M. P., Methyl-based NMR spectroscopy methods for uncovering structural dynamics in large proteins and protein complexes. *Biochemistry* **2018,** *58* (3), 144-155.
11. Tugarinov, V.; Kanelis, V.; Kay, L. E., Isotope labeling strategies for the study of high-molecular-weight proteins by solution NMR spectroscopy. *Nat. Protoc.* **2006,** *1* (2), 749-754.
12. Otten, R.; Chu, B.; Krewulak, K. D.; Vogel, H. J.; Mulder, F. A., Comprehensive and cost-effective NMR spectroscopy of methyl groups in large proteins. *J. Am. Chem. Soc.* **2010,** *132* (9), 2952-2960.
13. Kerfah, R.; Plevin, M. J.; Sounier, R.; Gans, P.; Boisbouvier, J., Methyl-specific isotopic labeling: a molecular tool box for solution NMR studies of large proteins. *Curr. Opin. Struct. Biol.* **2015,** *32*, 113-122.
14. Muhandiram, D.; Yamazaki, T.; Sykes, B. D.; Kay, L. E., Measurement of 2H T1 and T1ρ Relaxation times in uniformly 13C-labeled and fractionally 2H-labeled proteins in solution. *J. Am. Chem. Soc.* **1995,** *117* (46), 11536-11544.
15. Millet, O.; Muhandiram, D.; Skrynnikov, N. R.; Kay, L. E., Deuterium spin probes of side-chain dynamics in proteins. 1. Measurement of five relaxation rates per deuteron in 13C-

labeled and fractionally 2H-enriched proteins in solution. *J. Am. Chem. Soc.* **2002,** *124* (22), 6439-6448.

16. Tugarinov, V.; Ollerenshaw, J. E.; Kay, L. E., Probing side-chain dynamics in high molecular weight proteins by deuterium NMR spin relaxation: an application to an 82-kDa enzyme. *J. Am. Chem. Soc.* **2005,** *127* (22), 8214-8225.
17. Liao, X.; Long, D.; Li, D.-W.; Brüschweiler, R.; Tugarinov, V., Probing side-chain dynamics in proteins by the measurement of nine deuterium relaxation rates per methyl group. *J. Phys. Chem. B* **2012,** *116* (1), 606-620.
18. Tugarinov, V.; Kay, L. E., Relaxation rates of degenerate 1H transitions in methyl groups of proteins as reporters of side-chain dynamics. *J. Am. Chem. Soc.* **2006,** *128* (22), 7299-7308.
19. Tugarinov, V.; Sprangers, R.; Kay, L. E., Probing side-chain dynamics in the proteasome by relaxation violated coherence transfer NMR spectroscopy. *J. Am. Chem. Soc.* **2007,** *129* (6), 1743-1750.
20. Tugarinov, V.; Karamanos, T. K.; Clore, G. M., Magic-angle-pulse driven separation of degenerate 1H transitions in methyl groups of proteins: application to studies of methyl axis dynamics. *ChemPhysChem* **2020,** *21* (11), 1087-1091.
21. Nicholson, L. K.; Kay, L. E.; Baldisseri, D. M.; Arango, J.; Young, P. E.; Bax, A.; Torchia, D. A., Dynamics of methyl groups in proteins as studied by proton-detected carbon-13 NMR spectroscopy. Application to the leucine residues of staphylococcal nuclease. *Biochemistry* **1992,** *31* (23), 5253-5263.
22. Lee, A. L.; Flynn, P. F.; Wand, A. J., Comparison of 2H and 13C NMR relaxation techniques for the study of protein methyl group dynamics in solution. *J. Am. Chem. Soc.* **1999,** *121* (12), 2891-2902.
23. Ishima, R.; Petkova, A. P.; Louis, J. M.; Torchia, D. A., Comparison of methyl rotation axis order parameters derived from model-free analyses of 2H and 13C longitudinal and transverse relaxation rates measured in the same protein sample. *J. Am. Chem. Soc.* **2001,** *123* (25), 6164-6171.
24. Liu, W.; Zheng, Y.; Cistola, D. P.; Yang, D., Measurement of methyl 13C-1H cross-correlation in uniformly 13C-, 15N-, labeled proteins. *J. Biomol. NMR* **2003,** *27* (4), 351-364.
25. Zhang, X.; Sui, X.; Yang, D., Probing methyl dynamics from 13C autocorrelated and cross-correlated relaxation. *J. Am. Chem. Soc.* **2006,** *128* (15), 5073-81.
26. Brath, U.; Akke, M.; Yang, D.; Kay, L. E.; Mulder, F. A., Functional dynamics of human FKBP12 revealed by methyl 13C rotating frame relaxation dispersion NMR spectroscopy. *J. Am. Chem. Soc.* **2006,** *128* (17), 5718-5727.
27. Weininger, U.; Blissing, A. T.; Hennig, J.; Ahlner, A.; Liu, Z.; Vogel, H. J.; Akke, M.; Lundström, P., Protein conformational exchange measured by 1H R1ρ relaxation dispersion of methyl groups. *J. Biomol. NMR* **2013,** *57* (1), 47-55.
28. Mulder, F. A.; Hon, B.; Mittermaier, A.; Dahlquist, F. W.; Kay, L. E., Slow internal dynamics in proteins: application of NMR relaxation dispersion spectroscopy to methyl groups in a cavity mutant of T4 lysozyme. *J. Am. Chem. Soc.* **2002,** *124* (7), 1443-1451.

29. Tugarinov, V.; Kay, L. E., Separating degenerate 1H transitions in methyl group probes for single-quantum 1H-CPMG relaxation dispersion NMR spectroscopy. *J. Am. Chem. Soc.* **2007,** *129* (30), 9514-9521.

30. Otten, R.; Villali, J.; Kern, D.; Mulder, F. A., Probing microsecond time scale dynamics in proteins by methyl 1H Carr−Purcell−Meiboom−Gill relaxation dispersion NMR measurements. Application to activation of the signaling protein NtrCr. *J. Am. Chem. Soc.* **2010,** *132* (47), 17004-17014.

31. Hansen, A. L.; Lundström, P.; Velyvis, A.; Kay, L. E., Quantifying millisecond exchange dynamics in proteins by CPMG relaxation dispersion NMR using side-chain 1H probes. *J. Am. Chem. Soc.* **2012,** *134* (6), 3178-3189.

32. Bouvignies, G.; Kay, L. E., A 2D 13C-CEST experiment for studying slowly exchanging protein systems using methyl probes: An application to protein folding. *J. Biomol. NMR* **2012,** *53* (4), 303-310.

33. Yuwen, T.; Huang, R.; Kay, L. E., Probing slow timescale dynamics in proteins using methyl 1H CEST. *J. Biomol. NMR* **2017,** *68* (3), 215-224.

34. Chou, J. J.; Case, D. A.; Bax, A., Insights into the mobility of methyl-bearing side chains in proteins from 3JCC and 3JCN couplings. *J. Am. Chem. Soc.* **2003,** *125* (29), 8959-8966.

35. Pritchard, R. B.; Hansen, D. F., Characterising side chains in large proteins by protonless 13C-detected NMR spectroscopy. *Nat. Commun.* **2019,** *10* (1), 1-7.

36. Fares, C.; Lakomek, N.-A.; Walter, K. F.; Frank, B. T.; Meiler, J.; Becker, S.; Griesinger, C., Accessing ns–μs side chain dynamics in ubiquitin with methyl RDCs. *J. Biomol. NMR* **2009,** *45* (1-2), 23-44.

37. Agarwal, V.; Xue, Y.; Reif, B.; Skrynnikov, N. R., Protein side-chain dynamics as observed by solution-and solid-state NMR spectroscopy: a similarity revealed. *J. Am. Chem. Soc.* **2008,** *130* (49), 16611-16621.

38. Vugmeyster, L.; Ostrovsky, D.; Ford, J. J.; Burton, S. D.; Lipton, A. S.; Hoatson, G. L.; Vold, R. L., Probing the dynamics of a protein hydrophobic core by deuteron solid-state nuclear magnetic resonance spectroscopy. *J. Am. Chem. Soc.* **2009,** *131* (38), 13651-13658.

39. Busi, B.; Yarava, J. R.; Hofstetter, A.; Salvi, N.; Cala-De Paepe, D.; Lewandowski, J. z. R.; Blackledge, M.; Emsley, L., Probing Protein Dynamics Using Multifield Variable Temperature NMR Relaxation and Molecular Dynamics Simulation. *J. Phys. Chem. B* **2018,** *122* (42), 9697-9702.

40. Mao, J.; Aladin, V.; Jin, X.; Leeder, A. J.; Brown, L. J.; Brown, R. C.; He, X.; Corzilius, B. r.; Glaubitz, C., Exploring protein structures by DNP-enhanced methyl solid-state NMR spectroscopy. *J. Am. Chem. Soc.* **2019,** *141* (50), 19888-19901.

41. Xie, M.; Yu, L.; Bruschweiler-Li, L.; Xiang, X.; Hansen, A. L.; Brüschweiler, R., Functional protein dynamics on uncharted time scales detected by nanoparticle-assisted NMR spin relaxation. *Sci. Adv.* **2019,** *5* (8), eaax5560.

42. Wardenfelt, S.; Xiang, X.; Xie, M.; Yu, L.; Bruschweiler-Li, L.; Brüschweiler, R., Broadband dynamics of ubiquitin by anionic and cationic nanoparticle assisted NMR spin relaxation. *Angew. Chem., Int. Ed.* **2021,** *60* (1), 148-152.

43. Zhang, B.; Xie, M.; Bruschweiler-Li, L.; Bingol, K.; Brüschweiler, R., Use of charged nanoparticles in NMR-based metabolomics for spectral simplification and improved metabolite identification. *Anal. Chem.* **2015,** *87* (14), 7211-7217.

44. Cornilescu, G.; Marquardt, J. L.; Ottiger, M.; Bax, A., Validation of protein structure from anisotropic carbonyl chemical shifts in a dilute liquid crystalline phase. *J. Am. Chem. Soc.* **1998,** *120* (27), 6836-6837.

45. Senn, H.; Werner, B.; Messerle, B.; Weber, C.; Traber, R.; Wüthrich, K., Stereospecific assignment of the methyl 1H NMR lines of valine and leucine in polypeptides by nonrandom 13C labelling. *FEBS Lett.* **1989,** *249* (1), 113-118.

46. Delaglio, F.; Grzesiek, S.; Vuister, G. W.; Zhu, G.; Pfeifer, J.; Bax, A., NMRPipe: a multidimensional spectral processing system based on UNIX pipes. *J. Biomol. NMR* **1995,** *6* (3), 277-293.

47. Lee, W.; Tonelli, M.; Markley, J. L., NMRFAM-SPARKY: enhanced software for biomolecular NMR spectroscopy. *Bioinformatics* **2015,** *31* (8), 1325-1327.

48. Jacobsen, J. P.; Bildsøe, H. K.; Schaumburg, K., Application of density matrix formalism in NMR spectroscopy. II. The one-spin-1 case in anisotropic phase. *J. Magn. Reson.* **1976,** *23* (1), 153-164.

49. Vold, R. R.; Vold, R. L., Deuterium relaxation of chloroform dissolved in a nematic liquid crystal. *J. Chem. Phys.* **1977,** *66* (9), 4018-4024.

50. Mittermaier, A.; Kay, L. E., Measurement of methyl 2H quadrupolar couplings in oriented proteins. How uniform is the quadrupolar coupling constant? *J. Am. Chem. Soc.* **1999,** *121* (45), 10608-10613.

51. Clore, G. M.; Szabo, A.; Bax, A.; Kay, L. E.; Driscoll, P. C.; Gronenborn, A. M., Deviations from the simple two-parameter model-free approach to the interpretation of nitrogen-15 nuclear magnetic relaxation of proteins. *J. Am. Chem. Soc.* **1990,** *112* (12), 4989-4991.

52. Lipari, G.; Szabo, A., Model-free approach to the interpretation of nuclear magnetic resonance relaxation in macromolecules. 1. Theory and range of validity. *J. Am. Chem. Soc.* **1982,** *104* (17), 4546-4559.

53. Skrynnikov, N. R.; Millet, O.; Kay, L. E., Deuterium spin probes of side-chain dynamics in proteins. 2. Spectral density mapping and identification of nanosecond time-scale side-chain motions. *J. Am. Chem. Soc.* **2002,** *124* (22), 6449-6460.

54. Showalter, S. A.; Johnson, E.; Rance, M.; Brüschweiler, R., Toward quantitative interpretation of methyl side-chain dynamics from NMR by molecular dynamics simulations. *J. Am. Chem. Soc.* **2007,** *129* (46), 14146-14147.

55. Esadze, A.; Li, D.-W.; Wang, T.; Brüschweiler, R.; Iwahara, J., Dynamics of lysine side-chain amino groups in a protein studied by heteronuclear 1H−15N NMR spectroscopy. *J. Am. Chem. Soc.* **2011,** *133* (4), 909-919.

56. Abraham, M. J.; Murtola, T.; Schulz, R.; Páll, S.; Smith, J. C.; Hess, B.; Lindahl, E., GROMACS: High performance molecular simulations through multi-level parallelism from laptops to supercomputers. *SoftwareX* **2015,** *1*, 19-25.

57. Yu, L.; Li, D.-W.; Brüschweiler, R., Balanced amino-acid-specific molecular dynamics force field for the realistic simulation of both folded and disordered proteins. *J. Chem. Theory Comput.* **2019,** *16* (2), 1311-1318.

58. Jorgensen, W. L.; Chandrasekhar, J.; Madura, J. D.; Impey, R. W.; Klein, M. L., Comparison of simple potential functions for simulating liquid water. *J. Chem. Phys.* **1983,** *79* (2), 926-935.

59. Gu, Y.; Li, D.-W.; Brüschweiler, R., NMR order parameter determination from long molecular dynamics trajectories for objective comparison with experiment. *J. Chem. Theory Comput.* **2014,** *10* (6), 2599-2607.

60. Jameson, G.; Brüschweiler, R., NMR spin relaxation theory of biomolecules undergoing highly asymmetric exchange with large interaction partners. *J. Chem. Theory Comput.* **2021**.

61. Ester, M.; Kriegel, H.-P.; Sander, J.; Xu, X., A density-based algorithm for discovering clusters in large spatial databases with noise. *Kdd* **1996,** *96* (34), 226-231.

62. Ming, D.; Brüschweiler, R., Prediction of methyl-side chain dynamics in proteins. *J. Biomol. NMR* **2004,** *29* (3), 363-368.

63. Makhatadze, G. I.; Lopez, M. M.; Richardson III, J. M.; Thmos, S. T., Anion binding to the ubiquitin molecule. *Protein Sci.* **1998,** *7* (3), 689-697.

64. Zuin, A.; Isasa, M.; Crosas, B., Ubiquitin signaling: extreme conservation as a source of diversity. *Cells* **2014,** *3* (3), 690-701.

65. Schneider, D. M.; Dellwo, M. J.; Wand, A. J., Fast internal main-chain dynamics of human ubiquitin. *Biochemistry* **1992,** *31* (14), 3645-3652.

66. Lienin, S.; Bremi, T.; Brutscher, B.; Brüschweiler, R.; Ernst, R., Anisotropic intramolecular backbone dynamics of ubiquitin characterized by NMR relaxation and MD computer simulation. *J. Am. Chem. Soc.* **1998,** *120* (38), 9870-9879.

67. Chang, S.-L.; Tjandra, N., Temperature dependence of protein backbone motion from carbonyl 13C and amide 15N NMR relaxation. *J. Magn. Reson.* **2005,** *174* (1), 43-53.

68. Smith, C. A.; Ban, D.; Pratihar, S.; Giller, K.; Paulat, M.; Becker, S.; Griesinger, C.; Lee, D.; de Groot, B. L., Allosteric switch regulates protein–protein binding through collective motion. *Proc. Natl. Acad. Sci. U. S. A.* **2016,** *113* (12), 3269-3274.

69. Cousin, S. F.; Kadeřávek, P.; Bolik-Coulon, N.; Gu, Y.; Charlier, C.; Carlier, L.; Bruschweiler-Li, L.; Marquardsen, T.; Tyburn, J.-M.; Brüschweiler, R.; Ferrage, F., Time-resolved protein side-chain motions unraveled by high-resolution relaxometry and molecular dynamics simulations. *J. Am. Chem. Soc.* **2018,** *140* (41), 13456-13465.

70. Bolik-Coulon, N.; Kadeřávek, P.; Pelupessy, P.; Dumez, J.-N.; Ferrage, F.; Cousin, S. F., Theoretical and computational framework for the analysis of the relaxation properties of arbitrary spin systems. Application to high-resolution relaxometry. *J. Magn. Reson.* **2020,** *313*, 106718.

71. Schanda, P.; Huber, M.; Boisbouvier, J.; Meier, B. H.; Ernst, M., Solid-State NMR Measurements of Asymmetric Dipolar Couplings Provide Insight into Protein Side-Chain Motion. *Angew. Chem., Int. Ed.* **2011,** *50* (46), 11005-11009.

72. Haller, J. D.; Schanda, P., Amplitudes and time scales of picosecond-to-microsecond motion in proteins studied by solid-state NMR: a critical evaluation of experimental approaches and application to crystalline ubiquitin. *J. Biomol. NMR* **2013,** *57* (3), 263-280.

73. Ko, T.-P.; Liao, C.-C.; Ku, W.-Y.; Chak, K.-F.; Yuan, H. S., The crystal structure of the DNase domain of colicin E7 in complex with its inhibitor Im7 protein. *Structure* **1999,** *7* (1), 91-102.

74. Housden, N. G.; Kleanthous, C., Thermodynamic dissection of colicin interactions. *Methods Enzymol.* **2011,** *488*, 123-145.

75. Whittaker, S. B. M.; Clayden, N. J.; Moore, G. R., NMR characterisation of the relationship between frustration and the excited state of Im7. *J. Mol. Biol.* **2011,** *414* (4), 511-529.

76. Yang, D.; Kay, L. E., The effects of cross correlation and cross relaxation on the measurement of deuterium T1 and T1ρ relaxation times in 13CH2D spin systems. *J. Magn. Reson., Ser. B* **1996,** *2* (110), 213-218.

77. Li, D.-W.; Brüschweiler, R., A dictionary for protein side-chain entropies from NMR order parameters. *J. Am. Chem. Soc.* **2009,** *131* (21), 7226-7227.

78. Towse, C.-L.; Akke, M.; Daggett, V., The dynameomics entropy dictionary: a large-scale assessment of conformational entropy across protein fold space. *J. Phys. Chem. B* **2017,** *121* (16), 3933-3945.

79. Wand, A. J.; Sharp, K. A., Measuring entropy in molecular recognition by proteins. *Annu. Rev. Biophys.* **2018,** *47*, 41-61.

80. Klepeis, J. L.; Lindorff-Larsen, K.; Dror, R. O.; Shaw, D. E., Long-timescale molecular dynamics simulations of protein structure and function. *Curr. Opin. Struct. Biol.* **2009,** *19* (2), 120-127.

81. Long, D.; Li, D.-W.; Walter, K. F.; Griesinger, C.; Brüschweiler, R., Toward a predictive understanding of slow methyl group dynamics in proteins. *Biophys. J.* **2011,** *101* (4), 910-915.

82. O'Brien, E. S.; Wand, A. J.; Sharp, K. A., On the ability of molecular dynamics force fields to recapitulate NMR derived protein side chain order parameters. *Protein Sci.* **2016,** *25* (6), 1156-1160.

83. Hoffmann, F.; Xue, M.; Schäfer, L. V.; Mulder, F. A., Narrowing the gap between experimental and computational determination of methyl group dynamics in proteins. *Phys. Chem. Chem. Phys.* **2018,** *20* (38), 24577-24590.

84. Hoffmann, F.; Mulder, F. A.; Schäfer, L. V., Predicting NMR relaxation of proteins from molecular dynamics simulations with accurate methyl rotation barriers. *J. Chem. Phys.* **2020,** *152* (8), 084102.

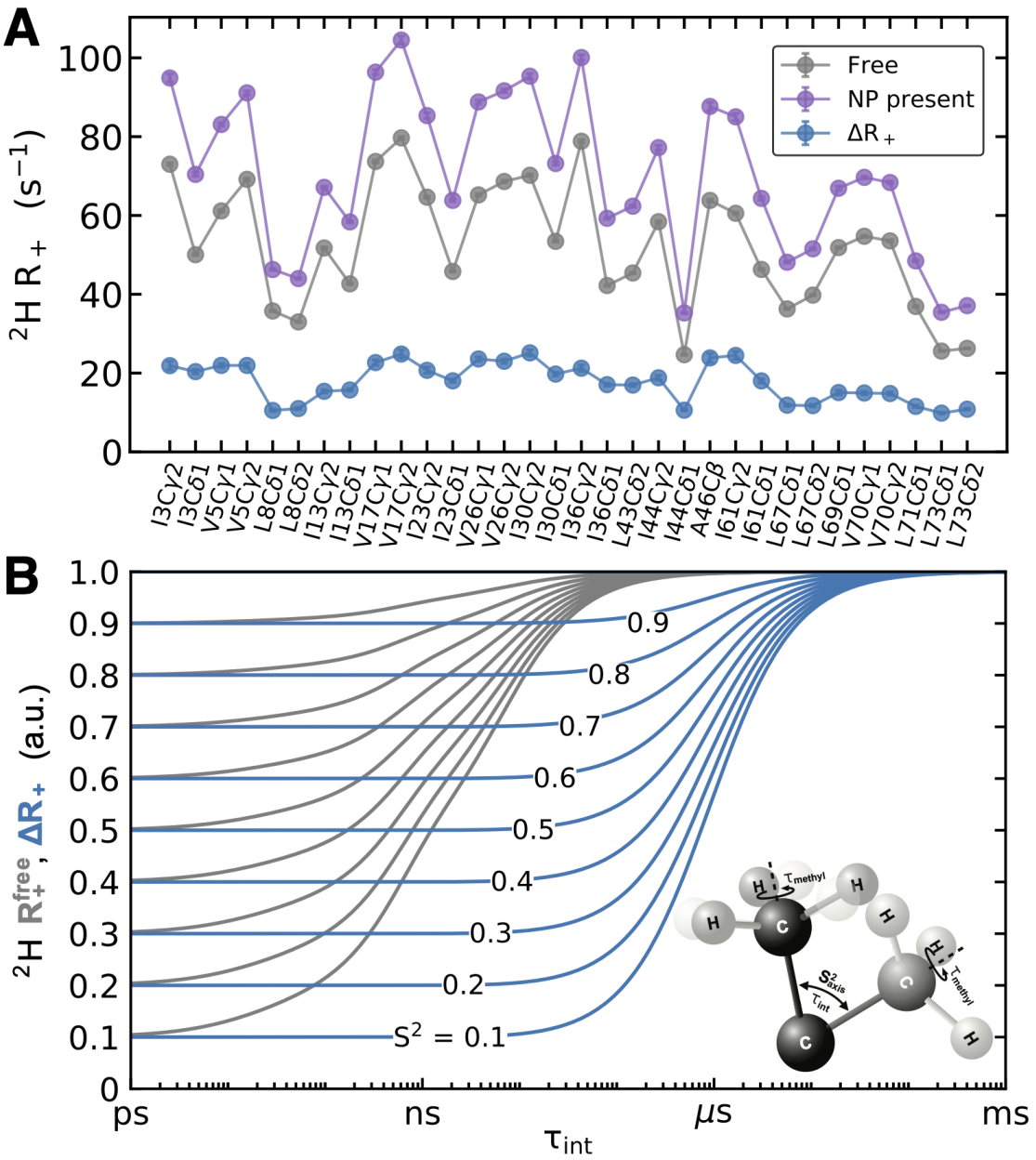

Figure 1. Experimental ^{2}H-methyl transverse spin relaxation rates R_+ in the presence and absence of nanoparticles and simulated dependence of ΔR_+ on the timescales of internal motions. **(A)** Ubiquitin ^{2}H transverse relaxation rates R_+ of methyl $^{13}CH_2D$ groups measured in the absence (grey, R_+^{free}) and in the presence (purple, R_+^{NP}) of 20 nm anionic SNPs. The blue circles correspond to their difference $\Delta R_+ = R_+^{NP} - R_+^{free}$. **(B)** Simulated dependence of R_+^{free} (gray) and ΔR_+ (blue) on the internal correlation time τ_{int} and motional amplitude S^2_{axis} of the methyl group rotation axis (C-C bond vector). The protein rotational correlation time τ_P was set to 5 ns, the correlation time τ_{methyl} for rapid methyl group rotation was set to 20 ps and the NP size was set to 20 nm, which corresponds to τ_{NP} = 0.91 μs according to the Stokes-Einstein-Debye relationship. R_+ and ΔR_+ were normalized to maximal values of 1.0. ^{2}H-ΔR_+ extends the accessible timescales of internal motions into the μs range. Predicted methyl dipole-dipole cross-correlation ^{13}C-ΔΓ rates possess the same timescale dependence as ^{2}H-ΔR_+ shown in Panel B.

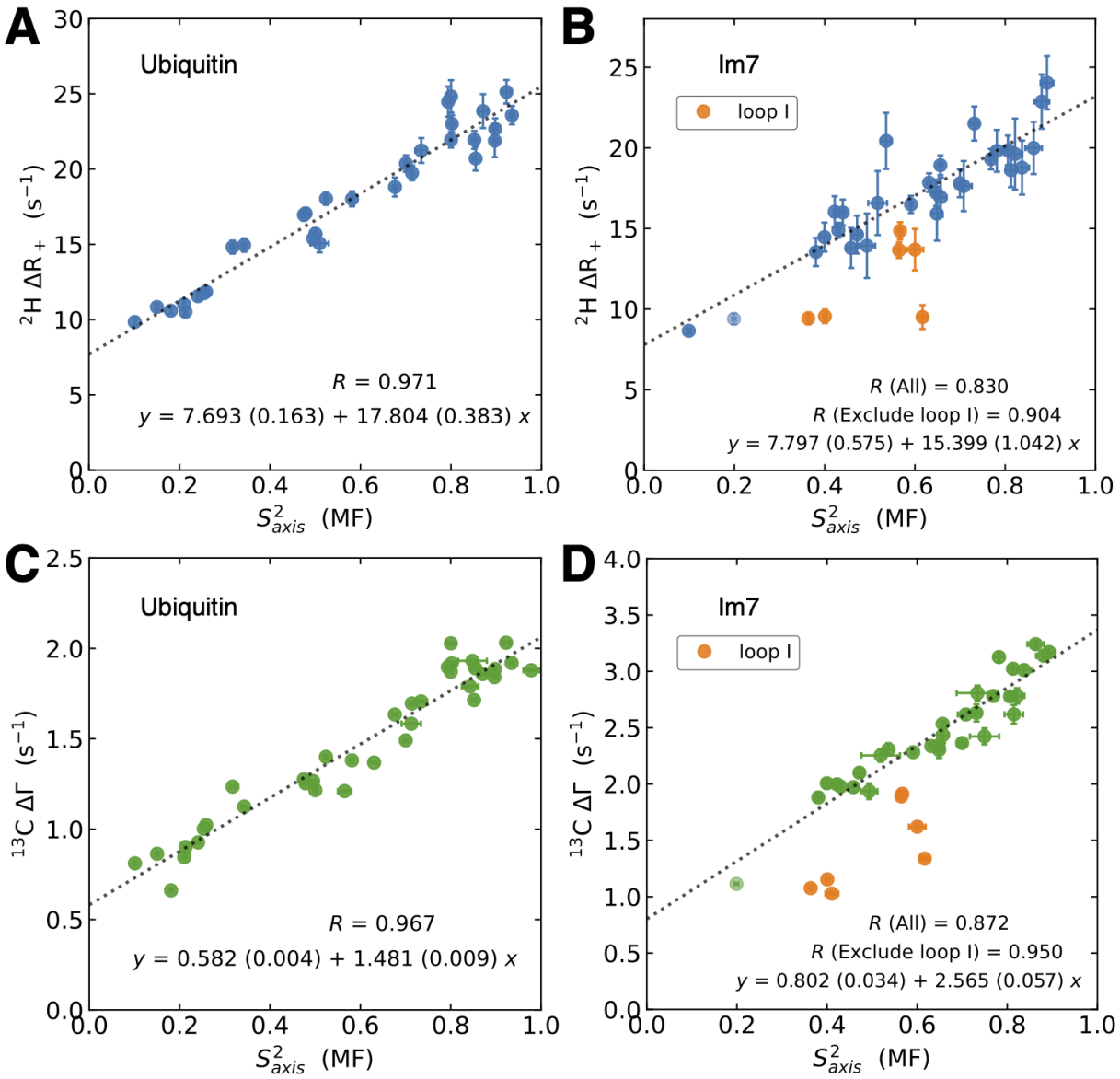

Figure 2. Comparison of methyl group dynamics probed by NASR measurements and standard model-free analysis (MF). **(A,B)** Correlation plot between S^2_{axis} (MF) (x-axis) and ^{2}H-ΔR_+ rates (y-axis) measured at 850 MHz of $^{13}CH_2D$ moieties of uniformly ^{13}C, partially ^{2}H labeled **(A)** ubiquitin and **(B)** Im7 using 20 nm SNPs. **(C,D)** Correlation plot between S^2_{axis} (MF) (x-axis) and ^{13}C-$\Delta\Gamma$ rates (y-axis) measured for $^{13}CH_3$ groups of uniformly ^{13}C labeled, fully protonated **(C)** ubiquitin and **(D)** Im7. In all panels, the standard model-free order parameters S^2_{axis} (MF) are derived from ^{2}H relaxation rates of $^{13}CH_2D$ groups: R_+, $R(D_z)$, and $R(3D_z^2 - 2)$. The Pearson correlation coefficients R and linear regression parameters are displayed in the plots with statistical uncertainties indicated in parentheses as determined by Monte Carlo simulations. Ala Cβ in the N-terminus SNA tag, which is a non-native residue in the Im7 construct used, is indicated with a lighter color in Panels B,D. The methyl-bearing residues of loop I of Im7, highlighted in orange, show a clear deviation from the linear relationship and their removal increases the Pearson correlation coefficients indicated in the figures. For the linear regressions (dotted lines) of Im7, the methyl groups in loop I were excluded.

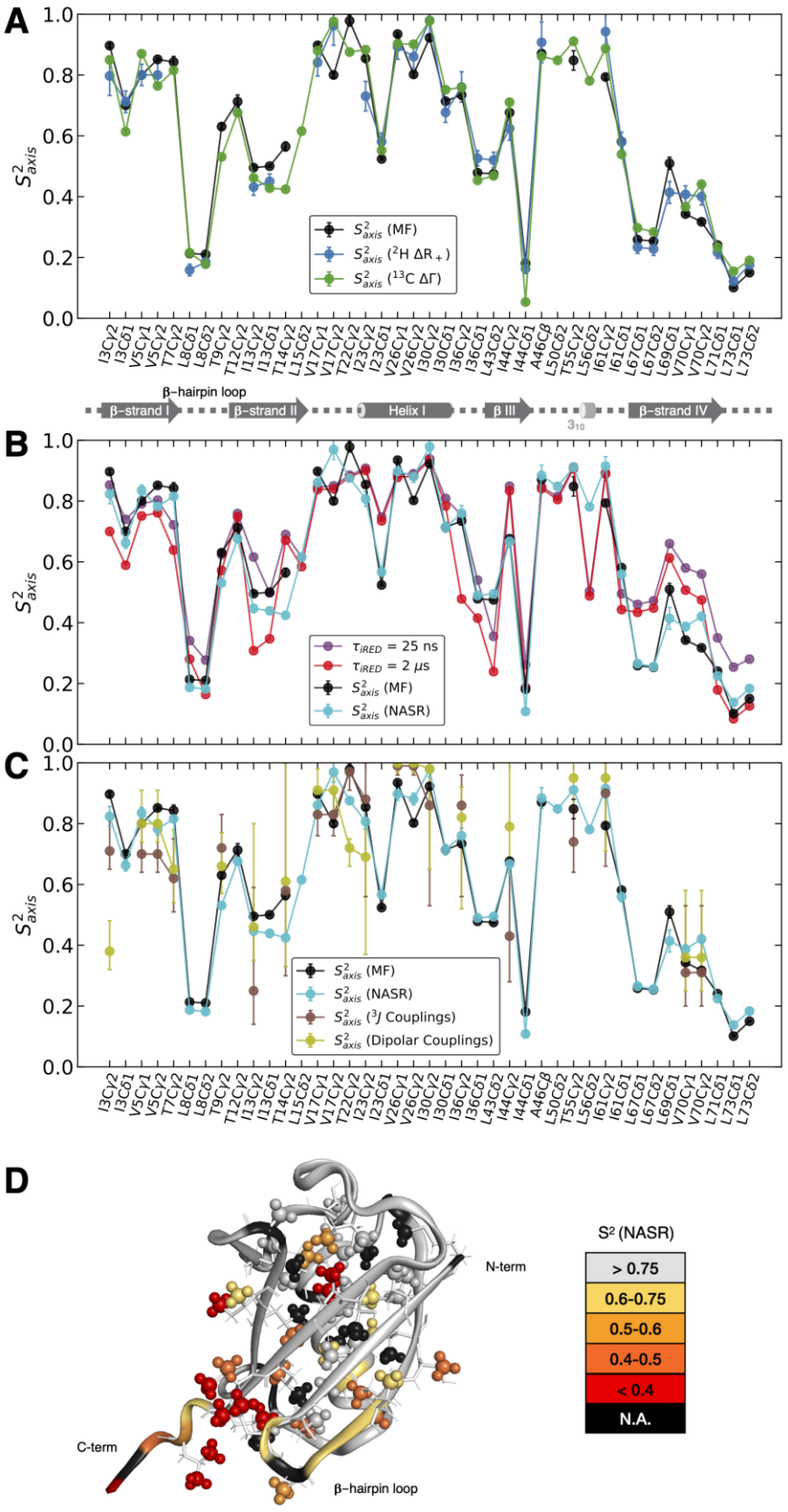
A
B
C
D
S^2_{axis}
S^2_{axis} (MF)
S^2_{axis} (^{2}H ΔR_+)
S^2_{axis} (^{13}C $\Delta\Gamma$)
β–hairpin loop
β–strand I
β–strand II
Helix I
β III
3_{10}
β–strand IV
τ_{iRED} = 25 ns
τ_{iRED} = 2 μs
S^2_{axis} (NASR)
S^2_{axis} (^3J Couplings)
S^2_{axis} (Dipolar Couplings)
I3Cγ2 I3Cδ1 V5Cγ1 V5Cγ2 T7Cγ2 L8Cδ1 L8Cδ2 T9Cγ2 T12Cγ2 I13Cγ2 I13Cδ1 T14Cγ2 L15Cδ2 V17Cγ1 V17Cγ2 T22Cγ2 I23Cγ2 I23Cδ1 V26Cγ1 V26Cγ2 I30Cγ2 I30Cδ1 I36Cγ2 I36Cδ1 L43Cδ2 I44Cγ2 I44Cδ1 A46Cβ L50Cδ2 T55Cγ2 L56Cδ2 I61Cγ2 I61Cδ1 L67Cδ1 L67Cδ2 L69Cδ1 V70Cγ1 V70Cγ2 L71Cδ1 L73Cδ1 L73Cδ2
N-term
C-term
β–hairpin loop
S² (NASR)
> 0.75
0.6-0.75
0.5-0.6
0.4-0.5
< 0.4
N.A.

Figure 3. Methyl-side chain dynamics of ubiquitin by NASR in comparison with other methods. **(A)** Comparison between ^{2}H-ΔR_+-derived $S^2_{\mathrm{axis}}\left(\,^{2}\mathrm{H}\,\Delta R_+\right)$ (blue), ^{13}C-ΔΓ-derived $S^2_{\mathrm{axis}}\left(^{13}\mathrm{C}\,\Delta\Gamma\right)$ (green) and standard model-free order parameters S^2_{axis} (MF) (black) where the secondary structure of ubiquitin is indicated at the bottom (β-strands as arrows and helices as cylinders). ^{2}H-ΔR_+ and ^{13}C- ΔΓ values were converted to S^2_{axis} values using the linear regression parameters of **Figure 2**. **(B)** Comparison of S^2_{axis} (NASR) (cyan) with S^2_{axis} (MF) (black) and S^2_{axis} determined from 10-μs MD trajectory with averaging time-windows τ_{iRED} = 25 ns and 2 μs (violet and red). S^2_{axis}(NASR) is the average of NASR-derived $S^2_{\mathrm{axis}}\left(\,^{2}\mathrm{H}\,\Delta R_+\right)$ and $S^2_{\mathrm{axis}}\left(^{13}\mathrm{C}\,\Delta\Gamma\right)$ values. **(C)** Comparison of S^2_{axis}(NASR) (cyan) with S^2_{axis}(MF) (black) and S^2_{axis} values derived from ^{3}J couplings (brown) and dipolar couplings (olive) in the literature (see main text). **(D)** S^2(NASR) values mapped on 3D structure of ubiquitin (PDB code 1UBQ). Methyl groups are represented as balls and sticks, which are colored according to S^2_{axis}(NASR), and the backbone ribbon is colored according to NASR ^{15}N-ΔR_2 derived S^2 values.

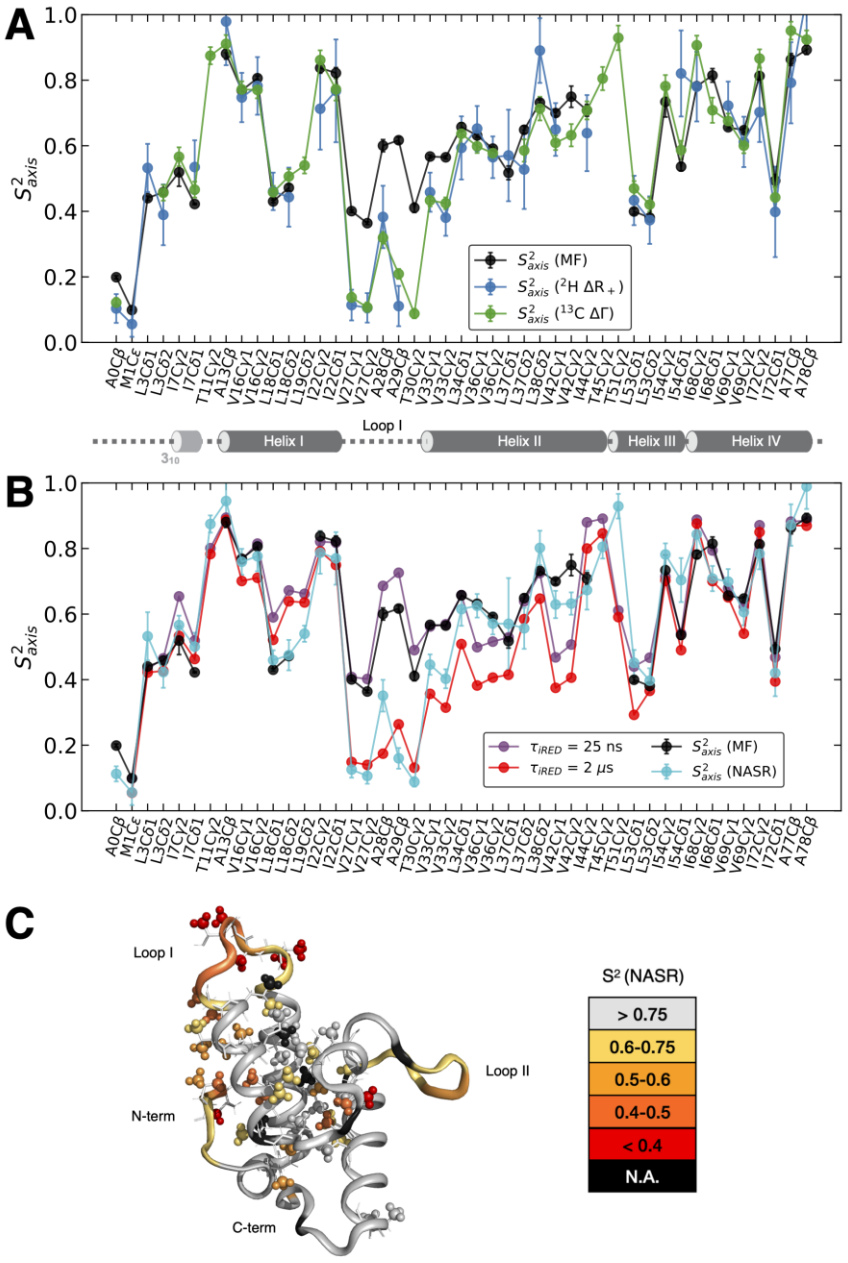

Figure 4. Methyl-side chain dynamics of Im7 by NASR in comparison with traditional ^{2}H-relaxation and MD results. **(A)** Comparison of NASR ^{2}H-ΔR_+-derived $S^2_{\text{axis}}\left(^2\text{H}\,\Delta R_+\right)$ (blue), NASR ^{13}C-ΔΓ-derived $S^2_{\text{axis}}\left(^{13}\text{C}\,\Delta\Gamma\right)$ (green) and the standard model-free order parameters S^2_{axis}(MF) (black) with secondary structure elements of Im7 indicated at the bottom (helices depicted as cylinders). ^{2}H-ΔR_+ and ^{13}C- ΔΓ values were converted to S^2_{axis} values using the linear regression parameters of **Figure 2**. **(B)** Comparison of S^2_{axis} (NASR) (cyan) and S^2_{axis} (MF) (black) with S^2_{axis} determined from 4-μs MD trajectory with averaging time-windows τ_{iRED} = 25 ns and 2 μs (violet and red). S^2_{axis}(NASR) is the average of NASR-derived $S^2_{\text{axis}}\left(^2\text{H}\,\Delta R_+\right)$ and $S^2_{\text{axis}}\left(^{13}\text{C}\,\Delta\Gamma\right)$ values. (**C**) S^2(NASR) values mapped on 3D structure of Im7 (PDB code 1CEI). Methyl groups are represented as balls and sticks, which are colored according to S^2_{axis}(NASR), and the backbone ribbon is colored according to NASR ^{15}N-ΔR_2 derived S^2 values.

TOC Figure

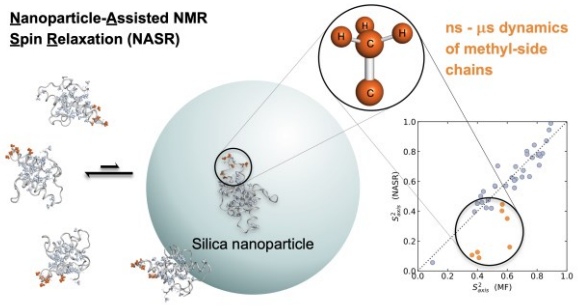
Nanoparticle-Assisted NMR
Spin Relaxation (NASR)
ns - μs dynamics
of methyl-side
chains
Silica nanoparticle
H
H
H
C
C
1.0
0.8
0.6
0.4
0.2
0.0
0.0
0.2
0.4
0.6
0.8
1.0
(NASR)
(MF)